Ground Wave Propagation Along an Inhomogeneous Rough Surface in the HF Band: Millington Effect for a Flat Earth

Christophe Bourlier and Gildas Kubické

***Abstract*—In this paper, for a vertically polarized line source in the high-frequency band (3–30 MHz), a detailed analysis of the ground wave propagation over 1-D highly conducting inhomogeneous (presence of island) smooth and rough surfaces is addressed from two methods: 1) the analytical solution of Bremmer (see also Wait), which assumes that the receiver, emitter, and island heights are zeros and that the surface is composed of three smooth paths of different permittivities, and 2) the efficient rigorous banded matrix iterative approach/canonical grid (BMIA-CAG) method, which is based on the method of moments and is updated to validate the analytical solution of Bremmer. In addition, from the works of Barrick, the sea surface roughness is included in the Bremmer formulation and tested from the BMIA-CAG by considering a surface composed of sea–land–sea mixed paths. The comparisons show a good agreement between the updated BMIA-CAG (reference method) and the Bremmer analytical formulation combined with the works of Barrick. The Earth curvature is neglected.**

***Index Terms*—Analytical models, electromagnetic modeling, radiowave propagation, rough surfaces, sea surface.**

I. Introduction

At HIGH frequencies (HFs) (3–30 MHz), the ground wave propagation is dominated by the surface wave. As long as the transmitter and receiver are close to the surface, direct and ground reflected waves cancel each other, and only the surface wave can propagate. The Earth's surface electrical parameters are important in reaching longer ranges. The sea surface is a very good conductor, but the land is a poor conductor at these frequencies. A challenging problem is to predict surface wave path loss variations over mixed paths, such as sea–land or sea–land–sea transitions. A sharp decrease in signal strength occurs along the sea–land transition, and the signal recovers itself beyond the island, known as the Millington (recovery) effect [1].

In the last century, many works were led to solve this issue. For a complete review of this problem, see the papers by Wait [2] and Collin [3] (and references therein) for a *homogeneous* smooth surface and the paper by Wait [2] for an *inhomogeneous* smooth surface. Recently, Bourlier *et al.* [4] have thoroughly studied the ground wave propagation over a 1-D *rough homogeneous* sea surface from an efficient rigorous numerical method: the method of moments (MoM) combined with the banded matrix iterative approach/canonical grid (BMIA-CAG) [5] and with the impedance boundary condition (IBC) (Leontovitch approximation). In addition, they compared, with the BMIA-CAG method, the closed-form asymptotic expression (the Sommerfeld solution of radiation of a vertically polarized line source above an infinite lossy half-space) of Collin [3], which is valid for a smooth surface and modified by the roughness from the works of Barrick [6], [7]. The comparisons were in good agreement for the emitter and receiver heights, which are small in comparison to the electromagnetic wavelength. As investigated in this paper, with a 1-D surface, we can solve a huge problem from the BMIA-CAG, typically ranging from 500 000 to 1 000 000 numbers of unknowns on the surface. This allows us to show, for the TM polarization, the ground wave propagation over a very long distance.

The purpose of this paper is to extend the study of Bourlier *et al.* to a 1-D *inhomogeneous rough* surface to predict the Millington recovery effect. The ground wave propagation above sea–land–sea mixed paths is then investigated by assuming a smooth sea surface and, next, by taking the sea surface roughness into account. Then, the BMIA-CAG reference method, valid for a *homogeneous* surface, is extended to an *inhomogeneous* surface. In addition, the Bremmer [8] analytical approach, valid for emitter, receiver, and island heights that are equal to zero, is tested, and from the works of Barrick [6], [7], an intuitive approach is proposed to take the surface roughness into account. In this paper, the curvature of the Earth is neglected, and the effect of the island shape is not investigated. These points will be investigated in a future study.

A similar study was published by Apaydin and Sevgi [9] (and references therein). First, in this paper, a very interesting review of the problem of the surface wave propagation along multimixed paths with irregular terrain over a spherical Earth is presented. In addition, a numerical method, based on a finite-element method [10], is presented to predict the propagation losses with duct effect over a spherical Earth in the presence of islands, and their algorithm is compared with the results computed from the Millington curve-fitting method [1], [11] tested in [12]. The surface roughness effect is not investigated.

This paper is organized as follows. Section II presents a review of the asymptotic solution of the ground wave

Manuscript received February 15, 2010; revised June 28, 2010 and September 6, 2010; accepted September 6, 2010. Date of publication October 28, 2010; date of current version March 25, 2011.

The authors are with the Institut de Recherche en Electrotechnique et Electronique de Nantes Atlantique Laboratory, Université Nantes Angers Le Mans, Polytech'Nantes, 44306 Nantes Cedex 3, France.

Color versions of one or more of the figures in this paper are available online at http://ieeexplore.ieee.org.

Digital Object Identifier 10.1109/TGRS.2010.2077302

propagation above an inhomogeneous smooth surface made up of three zones of different permittivities. In Section III, the BMIA-CAG method is briefly presented and updated to an inhomogeneous surface, and in Section IV, the analytical solution of Bremmer [8] is compared with the BMIA-CAG by taking the sea surface roughness into account. The last section gives the concluding remarks.

II. Analytic Solution

This section presents a closed-form expression of the attenuation function of the ground wave propagation above an inhomogeneous smooth surface made up of three sections of different permittivities.

To solve this issue, for an inhomogeneous smooth surface made up of two sections (land–sea or sea–land), the first analytical model was put forth by Millington [1] (read references therein for the history). It also predicts the recovery effect that occurs when the wave passes over a boundary from an area of poor conductivity (land) to one of good conductivity (sea). Millington does not provide a theoretical justification for his method, although he does indicate that his formulas for HFs are compatible with the expected behavior of the height-gain functions over the media on both sides of the boundary. Bremmer [8] formulated the problem in terms of an integral equation, which he solved by operational calculus. Bremmer considered several limiting cases and also established the validity of Millington's formulas at HFs. Wait [14], [15] also solved this problem by employing formalism based on the mutual impedance. For a complete review of this issue, see [2].

In this section, the Bremmer approach is reviewed. He started from the scalar integral equation of a 2-D surface and from a saddle point approximation [8], [13], and he converted the 2-D integral into a single integral. For a 1-D surface, using the same way as Bremmer, we then show in the Appendix that the integral equation satisfied by the attenuation function $F=\psi/(2\psi_i)$, in which ψ is the total field and ψ_i is the incident field of a line source, is

$$F(x,z)=1+\frac{j}{\sqrt{\pi}}\int_0^x F(\xi,z_\xi)\alpha(\xi)e^{jk_0(QR+TQ-TR)} \times\sqrt{\frac{TR}{QR\times TQ}}\left[1-\frac{\gamma_\xi(\xi-x)-(z_\xi-z)}{\Delta(\xi)\sqrt{1+\gamma_\xi^2}QR}\right] \times\sqrt{1+\gamma_\xi^2}\,d\xi \tag{1}$$

where

$$\alpha(\xi)=\Delta(\xi)\sqrt{\frac{jk_0}{2}}=\frac{1}{n(\xi)}\sqrt{1-\frac{1}{n^2(\xi)}}\sqrt{\frac{jk_0}{2}}. \tag{2}$$

The points $T(0,z_0)$, $Q(\xi,z_\xi)$, and $R(x,z)$ give the position of the transmitter, a point on the surface of slope $\gamma_\xi=dz_\xi/d\xi$, and the position of the receiver, respectively (see Fig. 1). The terms QR, TQ, and TR are the distances between two points expressed in (A11). The aforementioned equation is valid for $k_0QR\gg 1$, $k_0TQ\gg 1$, and $k_0TR\gg 1$ and assumes that the surface is highly conducting ($|\Delta|\ll 1$ or $|n|\gg 1$) to apply the Leontovitch boundary condition. Δ is the surface normalized impedance, which depends on ξ and surface refraction index n.

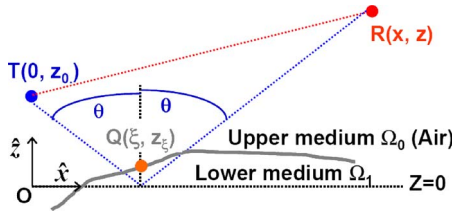

Fig. 1. Description of the geometry.

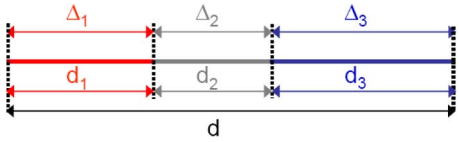

Fig. 2. Surface of length d made up of three sections of lengths $\{d_1,d_2,d_3\}$.

Assuming a flat Earth (the surface slope $\gamma_\xi=0\ \forall\ \xi$), the heights of the transmitter ($z_0=0$), receiver ($z=0$), and surface ($z_\xi=0$) are zero; from (A11), $QR=x-\xi$, $TQ=\xi$, and $TR=x$. Thus, (1) is simplified as

$$F(x)=1+j\sqrt{\frac{x}{\pi}}\int_0^x\frac{F(\xi)\alpha(\xi)}{\sqrt{\xi(x-\xi)}}\,d\xi \tag{3}$$

which is exactly the same equation obtained by Bremmer [8, eq. (11)].

For a homogeneous surface (subscript 1 for F), $\Delta(\xi)=\Delta$ is a constant with respect to ξ, and then, to solve the aforementioned integral equation, Bremmer [8] used operational calculus based on the Laplace transform and showed that

$$F_1(v)=1-\sqrt{\pi}ve^{v^2}erfc(v),\qquad v=\sqrt{\frac{k_0x}{2j}}\Delta \tag{4}$$

where $erfc$ is the complementary error function. Comparing this equation with the one obtained by Bourlier *et al.* [4] and calculated from the Collin formulation [3], the same equation is obtained if $|\Delta|\gg\chi$, where $\chi=\pi/2-\theta$ is the grazing angle (see Fig. 1). In fact, for $z+z_0\ll x$, $\chi\approx(z+z_0)/x$, and since we assumed that $z=z_0=0$, the condition $|\Delta|\gg\chi=0$ is satisfied.

Let us now consider a surface of length d made up of three sections of lengths $\{d_1,d_2,d_3\}$ with surface permittivities $\{\epsilon_{r1},\epsilon_{r2},\epsilon_{r3}\}\Rightarrow\{\Delta_1,\Delta_2,\Delta_3\}$ (see Fig. 2).

Bremmer showed for three sections (subscript 3 for F) that the attenuation function is given by (5), shown at the bottom of the next page, where

$$\Psi_2(\xi)=w_1(\xi)+\beta_{21}\int_{d_1}^{\xi}w_1(\xi_1)w_2(\xi-\xi_1)d\xi_1 \tag{6}$$

$$\beta_{nm}=j\frac{\alpha_n-\alpha_m}{\sqrt{\pi}} \tag{7}$$

in which

$$\alpha_n = \Delta_n \sqrt{\frac{jk_0}{2}} = \frac{jv_n}{\sqrt{x}}. \tag{8}$$

In addition, $w_n(x) = F_1(v_n)/\sqrt{x}$, in which $v_n = \sqrt{k_0 x/(2j)}\Delta_n$. For $x \in]d_1 + d_2; \infty[$, an alternative form of the last line of (5), which is more convenient for its numerical evaluation, can be found

$$\begin{aligned} F_3(x)/\sqrt{x} = {} & w_1(x) + \beta_{31} \int_{d_1+d_2}^{x} w_1(\xi) w_3(x-\xi)\, d\xi \\ & + \beta_{21} \int_{d_1}^{d_1+d_2} \Psi_2(\xi) w_1(\xi)\, d\xi, \qquad \text{for } x \in]d_1 + d_2; \infty[\end{aligned} \tag{9}$$

where

$$\Psi_2(\xi) = w_2(x-\xi) + \beta_{32} \int_{d_1+d_2}^{x} w_2(\xi_1 - \xi) w_3(x-\xi_1) d\xi_1. \tag{10}$$

Equation (5) shows that the addition of a section does not disturb the scattered field by the previous sections and that the attenuation function is expressed from the attenuation functions of a single section of surface normalized impedance Δ_n. If the surface is assumed to be homogeneous, then, for $x \in]d_1 + d_2; \infty[$, $F_3(x)/\sqrt{x} = w_3(x)$. Thus, in (5), for $x \in]d_1 + d_2; \infty[$, the terms after $w_3(x)$ can be interpreted as recovery integrals, corresponding to the Millington (recovery) effect.

III. Rigorous Numerical Method

This section presents a rigorous fast method based on the integral equations, which allows us to treat a very large problem. Indeed, to exhibit the ground wave, which propagates near the surface over a very large distance from the transmitter, the surface must be very large, typically a few hundreds of kilometers. For a frequency of the order of 10 MHz ($\lambda_0 = 30$ m) and with a sampling step of $\lambda_0/10 = 3$ m, the number of unknowns on the surface must then be greater than $N_i = 500\,000$.

As shown in [4], for a slightly *homogeneous* rough surface ($\sigma_z/\lambda_0 \ll 1$, where σ_z is the surface height standard deviation), the BMIA-CAG [5] is very efficient for our application. For a smooth surface, $\sigma_z = 0$. From a personal computer (4 GB of RAM and 3-GHz processor), the BMIA-CAG allows us to treat a very large problem up to $2^{20} = 1\,048\,576$ unknowns on the surface.

The BMIA-CAG is based on MoM [17]. Then, using MoM with point matching and pulse basis functions, a linear system $\bar{\mathbf{Z}}\mathbf{X} = \mathbf{b} \Rightarrow \mathbf{X} = \bar{\mathbf{Z}}^{-1}\mathbf{b}$ is obtained, in which $\bar{\mathbf{Z}}$ is the impedance matrix and $\mathbf{X}$ is the vector containing the unknowns sampled on the surface (currents). The elements of the impedance matrix can be found in [18]. Since the surface is assumed to be highly conducting ($|n| \gg 1$), the IBC (also named the Leontovitch boundary condition) approximation can be applied. For the TM polarization, this leads to $\partial\psi(\mathbf{r})/\partial n_s = -j\Delta k_0 \psi(\mathbf{r})$ on the surface, where Δ is the surface normalized impedance defined as $\Delta = \sqrt{1 - 1/n^2}/n$, $\psi(\mathbf{r})$ is the field on the surface, and $\partial\psi(\mathbf{r})/\partial n_s$ is the normal derivative of the field on the surface. The only unknown now is the field $\psi(\mathbf{r})$.

Moreover, since the number of unknowns N_i is huge, a classical LU (lower–upper) inversion cannot be applied to invert $\bar{\mathbf{Z}}$. The principle of BMIA-CAG is not to invert the impedance matrix but to replace $\bar{\mathbf{Z}}^{-1}\mathbf{b}$ by a succession of matrix–vector products. For more details, see [5] and [19]. This method then required the knowledge of two integers: 1) the width of the strong interaction band matrix $N_{s,\mathrm{BMIA}}$, which is much smaller than N_i, and 2) the term number P_{BMIA} retained in the series expansion of the impedance matrix elements of the weak interactions. Typically, for frequencies $f \in [10; 30]$ MHz and wind speeds $u_{10} \in [0; 10]$ m/s, N_i ranges from one to two, and P_{BMIA} ranges from one to three. Moreover, the integers $N_{s,\mathrm{BMIA}}$ and P_{BMIA} increase with the frequency and the wind speed.

In this paper, this method is updated by considering that the relative permittivity of the lower medium Ω_1 (see Fig. 1) $\epsilon_r(\xi)$ varies along the horizontal distance ξ. Under the IBC approximation, the skin depth $\delta_i = \lambda_0/[2\pi \mathrm{Im}(n_i)]$ of a section i is much smaller than the incident wavelength λ_0 because $|\mathrm{Im}(n_i)| \gg 1$. In the lower medium Ω_1, the field then damps very strongly against the vertical z. Thus, we assume in Ω_1 that the scattered fields of each section i of constant relative permittivity ϵ_{ri} do not interact between them. Considering this assumption, the impedance matrix of the MoM is modified, and we brought some changes in the algorithm of the BMIA-CAG to take into account the fact that $\epsilon_r(\xi)$ is a function of ξ.

IV. Numerical Results

In this section, in the HF band ($f \in [10; 30]$ MHz), the numerical results of the attenuation function are presented by considering a surface made up of three sections, as shown in Fig. 2. Sections 1 and 3 are smooth/rough surfaces, and section 2 is a smooth land. In addition, the emitter is located

$$F_3(x)/\sqrt{x} = \begin{cases} w_1(x), & \text{for } x \in [0; d_1] \\ w_2(x) + \beta_{12} \int_0^{d_1} w_1(\xi) w_2(x-\xi) d\xi, & \text{for } x \in]d_1; d_1 + d_2] \\ w_3(x) + \beta_{13} \int_0^{d_1} w_1(\xi) w_3(x-\xi) d\xi + \beta_{23} \int_{d_1}^{d_1+d_2} \Psi_2(\xi) w_3(x-\xi) d\xi, & \text{for } x \in]d_1 + d_2; \infty[\end{cases} \tag{5}$$

TABLE I
PARAMETERS USED FOR FIGS. 4–8 AND FOR THE CASE OF A SMOOTH SEA SURFACE WITH $z_0 = 10$ m AND $x_0 = 0$ m. THE SYMBOL "-" MEANS THAT THE CORRESPONDING PARAMETER CHANGES, AND IT IS GIVEN IN THE LEGEND OF THE CORRESPONDING FIGURE

Fig.	f (MHz)	z m	$(\epsilon'_{r2}, \sigma_2)$ (S/m,-)	h_2 m	d_2 km	d_1 km
4(a)	10	5	(-,-)	0	50	50
4(b)	30	5	(-,-)	0	50	50
5	10	5	(0.01,30)	0	-	50
6	10	5	(-,-)	0	50	100
7	-	5	(0.01,30)	0	50	50
8	30	40	(0.01,30)	-	50	50

at $(x_0, z_0) = (0, 10)$ m (abscissa of the surface center and $x \in [-L/2; L/2]$), and the number of unknowns on the surface is $N_i = 524\,288$, corresponding to a surface length of $L = N_i\lambda_0/10$ since the sampling step is $\lambda_0/10$. It should be noted that $x_{\max} = \max(x) = N_i\lambda_0/20 = \{786, 393, 262\}$ km for $f = \{10, 20, 30\}$ MHz.

The scattered field is derived from the field $\psi(\mathbf{r}')$, computed from the BMIA-CAG, and its normal derivative on the surface $\partial\psi(\mathbf{r}')/\partial n_s = -j\Delta k_0\psi(\mathbf{r}')$ by applying the Huygens principle defined as

$$\psi_s(\mathbf{r}) = \int_S \left[\frac{\partial g_0(\mathbf{r}, \mathbf{r}')}{\partial n_s}\psi(\mathbf{r}') - \frac{\partial\psi(\mathbf{r}')}{\partial n_s}g_0(\mathbf{r}, \mathbf{r}')\right] dS'. \quad (11)$$

The attenuation function is then computed from $\psi_s(\mathbf{r})$ as

$$F(\mathbf{r}) = \frac{\psi_s(\mathbf{r}) + \psi_i(\mathbf{r})}{2\psi_i(\mathbf{r})} = F(x, z) \quad (12)$$

where the incident field $\psi_i(\mathbf{r})$ is defined as

$$\psi_i(\mathbf{r}) = g_0(\mathbf{r}, \mathbf{r}_0) = \frac{j}{4}H_0^{(1)}\left(k_0\sqrt{(x - x_0)^2 + (z - z_0)^2}\right). \quad (13)$$

The complex relative permittivity ϵ_{ri} of section i is assumed to be

$$\epsilon_{ri} = \epsilon'_{ri} + \frac{j\sigma_i}{2\pi f\epsilon_0} = \epsilon'_{ri} + \frac{18j\sigma_i}{f(\text{GHz})} \quad (14)$$

where σ_i is the conductivity in siemens per meter and $n_i = \sqrt{\epsilon_{ri}}$. In addition, for the sea sections $(i = \{1, 3\})$, $\sigma_i = 4$ S/m, and the real part of the relative permittivity is $\epsilon'_{ri} = 80$, which implies that the sea complex relative permittivity is $\epsilon_{ri} = 80 + 72j/f$, with f in gigahertz. For the island (section 2), $(\epsilon'_{r2}, \sigma_2) = (30, 0.01$ S/m) for a very wet soil, whereas $(\epsilon'_{r2}, \sigma_2) = (15, 0.001$ S/m) for a wet soil.

A. Case of a Smooth Sea Surface

In this section, the sea surface is assumed to be smooth.

For Figs. 4–8, the parameters of the simulations are reported in Table I and are defined as follows.

1) f is the frequency in megahertz.
2) z is the height of the emitter in meters.

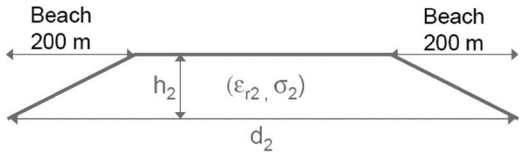

Fig. 3. Shape of the island (section 2) of real relative permittivity ϵ_{r2} and conductivity σ_2.

3) ϵ'_{r2} is the real relative permittivity of section 2 (island).
4) σ_2 is the conductivity of section 2 in siemens per meter.
5) h_2 is the height of the island in meters (see Fig. 3).
6) d_2 is the length of the island in kilometers.
7) d_1 is the abscissa of the beginning of the island in kilometers.

The island, shown in Fig. 3, has a trapezoidal shape, for which the beach lengths are 200 m. In the legend of each figure, the label "Num" means that F_3 is computed from the BMIA-CAG reference method, whereas the label "Ana" means that F_3 is computed from the Bremmer equation [see (5)].

As shown in Figs. 4–7, a very good agreement is obtained between the BMIA-CAG results and that obtained from the Bremmer equation. It is important to note that (5) is valid for $z = z_0 = 0$ m. For $f = 10$ MHz and $z_0 = 10$ m and since, in Figs. 4–7, $z = 5$ m, the ratio $(z + z_0)/\lambda_0 = 0.5$, which explains that the results match well.

Fig. 4 compares the case (full and cross curves) of a homogeneous surface $(\Delta_1 = \Delta_2 = \Delta_3)$ with a surface made up of three sections of surface normalized impedance $(\Delta_1, \Delta_2, \Delta_1)$ (sea-land-sea). Sections 1 and 3 are the seas, and section 2 is the island. As expected, a sharp decrease in the signal strength occurs along the sea–island transition, and the signal recovers itself after the island–sea transition (beyond the island), known as the Millington (recovery) effect. In addition, as the frequency increases (see also Fig. 7), the signal strength decreases more rapidly [the x and y scales are different in Fig. 4(a) and (b)], and the recovery effect is more important for $f = 30$ MHz.

As shown in Fig. 5, this effect occurs for any length d_2 of the island, and as shown in Fig. 6, this effect occurs for any electrical parameters (very wet or wet soils) of the island. In addition, as we can see in Fig. 6, the signal strength decreases more rapidly above a soil that is less wet.

As the island height increases, Fig. 8 shows that the signal strength weakly decreases above the island. In addition, the recovery effect varies slightly with the island height. However, in a recent study, Apaydin and Svegi [9] showed that the island shape (Gaussian and half-sinusoidal shapes are treated) can strongly disturb the Millington recovery effect.

In Fig. 8, the frequency is chosen as $f = 30$ MHz in order to have a ratio $h_2/\lambda_0 = \{0, 2, 3\}$ that is greater than one in terms of wavelength λ_0. Thus, Fig. 8 shows that the effect of the island height can be neglected for the propagation above the sea sections. For this configuration, the receiver height is chosen as $z = 40$ m $> h_2$, which explains that the results obtained from the Bremmer formulation do not coincide with that computed from the BMIA-CAG. In this case, the ratio $(z_0 + z)/\lambda_0 = 5$, which is not negligible in comparison to the

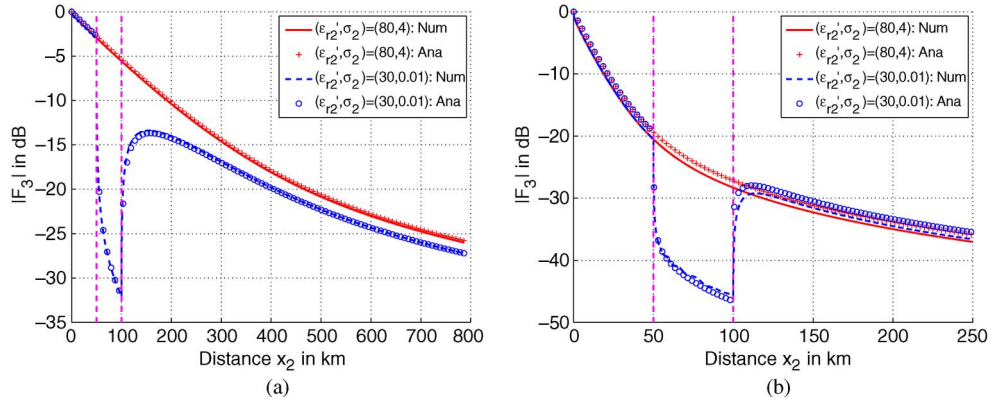

Fig. 4. $|F_3|$ versus the distance $x_2 = x - x_0$ in kilometers for a smooth sea surface. The parameters are given in Table I. The dashed vertical lines indicate the values of d_1 and $d_1 + d_2$. (a) $f = 10$ MHz. (b) $f = 30$ MHz.

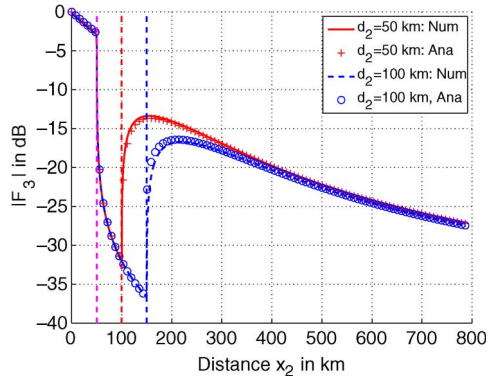

Fig. 5. Same as in Fig. 4.

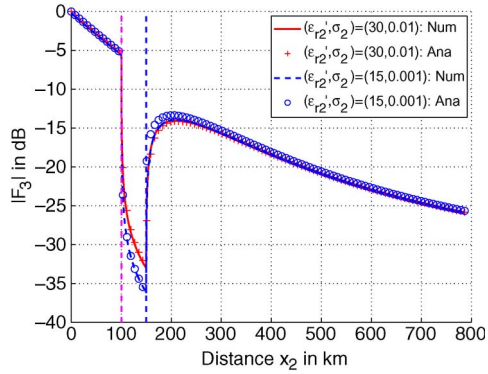

Fig. 6. Same as in Fig. 4.

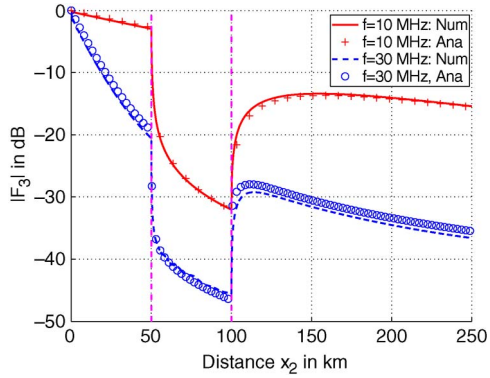

Fig. 7. Same as in Fig. 4.

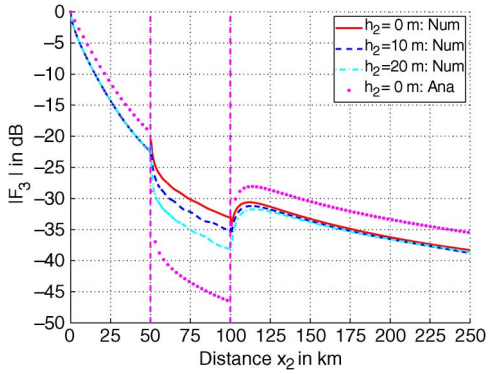

Fig. 8. Same as in Fig. 4.

wavelength. The difference is more important above the island because $1/|\Delta_{1,3}| < 1/|\Delta_2|$. Indeed, as the surface normalized impedance $|\Delta|$ decreases, the contribution of the second term between the brackets in (1) increases.

B. *Case of a Rough Sea Surface*

In this section, a rough sea surface is considered. The rough surface height is assumed to be a Gaussian stationary stochastic process with zero mean value, and the height spectrum obeys the hydrodynamic spectrum proposed by Elfouhaily *et al.* [21], in which the key parameter is the wind speed u_{10} at 10 m above the sea surface. In an electromagnetic point of view, in the HF band, since the ratio σ_z/λ_0 is much smaller than one, the surface is slightly rough. From the Elfouhaily spectrum, Bourlier and Berginc [16] showed that the height standard deviation is $\sigma_z \approx 6.29 \times 10^{-3} u_{10}^{2.02}$. For instance, for $u_{10} = 10$ m/s (Beaufort scale 6–7), $\sigma_z = 0.63$ m, which implies that the ratio $\sigma_z/\lambda_0 \in [0.021; 0.063]$ for $f \in [10; 30]$ MHz. Thus, the BMIA-CAG method is very efficient because its order P_{BMIA} and its strong interaction bandwidth $N_{s,\mathrm{BMIA}}$ are proportional to this ratio.

By using a spectral method, several independent surfaces (but with the same Gaussian process and the same height spectrum) are generated. For each surface numbered p, the field ψ_p and its normal derivative $\partial\psi_p/\partial n_s$ are computed, and then, from (11) and (12), the scattered field $\psi_{s,p}$ and the function $F_{3,p}$ are

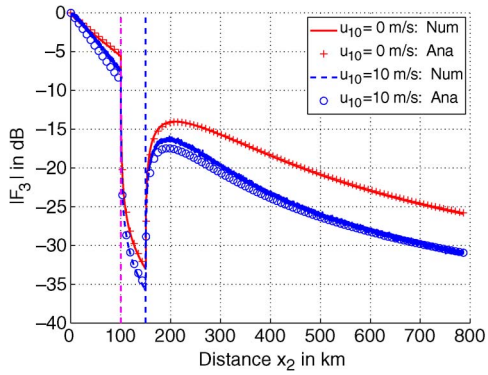

Fig. 9. $|F_3|$ versus the distance $x_2 = x - x_0$ in kilometers for a rough sea surface. The parameters are given in Table II. The dashed vertical lines indicate the values of d_1 and $d_1 + d_2$.

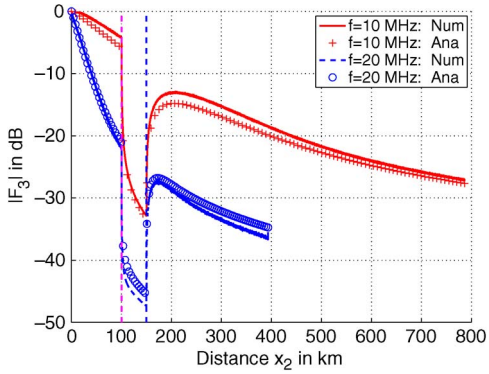

Fig. 10. Same as in Fig. 9.

computed. The average of F_3, denoted as $\langle F_3 \rangle$, is then obtained from

$$\langle F_3 \rangle = \frac{1}{N_r} \sum_{p=1}^{p=N_r} F_{3,p} \tag{15}$$

where N_r is the number of realizations.

From an asymptotic perturbative theory and assuming a homogeneous rough surface, Ishimaru *et al.* [20] showed that the coherent attenuation function $\langle F_1 \rangle$ keeps the same form as the one of a flat surface but with a new surface normalized impedance Δ^{rough} as a function of the smooth surface normalized impedance Δ^{flat} and of the sea roughness spectrum. In other words, $\Delta^{\text{rough}} \approx \Delta^{\text{flat}}(1 + a + jb)$, where $(a, b) \in \mathbb{R}^2$.

From the results computed from the BMIA-CAG, Bourlier *et al.* [4] investigated several methods to compute the real numbers a and b. They then showed that $a > 0$ and proportional to u_{10}^2, whereas $b < 0$ and $|b/a| \ll 1$. In addition, they compared a and b with those obtained from an analytical approach developed by Barrick [6], [7] and based on an asymptotic perturbative theory. A good agreement is then obtained between both methods.

To our knowledge, the approach developed for a smooth surface made up of three sections has not been generalized to the case of a rough surface. However, as the attenuation function F_3 depends on the attenuation functions of homogeneous sections, an intuitive way to take the roughness effect into account for sections 1 and 3 is to substitute the attenuation functions of sections 1 and 3 for the ones modified by the roughness. It is then equivalent to the substitution of the surface normalized impedance $\{\Delta_3^{\text{flat}} = \Delta_1^{\text{flat}}\}$ by Δ_1^{rough} computed from the Barrick formulation.

For Figs. 9 and 10, the parameters of the simulations are reported in Table II.

As the wind speed increases, Fig. 9 shows that the attenuation function decreases faster, and for a horizontal distance $x_2 = x - x_0 = 800$ km, the difference reaches 5 dB. The Millington effect also occurs for a rough sea surface. As we can see in Figs. 9 and 10, a good agreement is observed between the curves obtained from the Bremmer approach combined with the works of Barrick and the BMIA-CAG reference method.

TABLE II
PARAMETERS USED FOR FIGS. 9 AND 10 AND FOR THE CASE OF A ROUGH SEA SURFACE WITH $z_0 = 10$ m AND $x_0 = 0$ m. THE SYMBOL "-" MEANS THAT THE CORRESPONDING PARAMETER CHANGES, AND IT IS GIVEN IN THE LEGEND OF THE CORRESPONDING FIGURE. THE NUMBER OF REALIZATIONS IS $N_r = 10$

Fig.	f (MHz)	z m	$(\epsilon_{r2}, \sigma_2)$ (S/m,-)	h_2 m	d_2 km	d_1 km	u_{10} m/s
9	10	5	(0.01,30)	0	50	100	-
10	-	5	(0.01,30)	0	50	100	5

Indeed, the mean difference does not exceed 1 dB. Thus, the proposed approach to include the roughness is efficient.

C. Discussion on the Millington Effect

Equations (5) and (6) show for $x \in]d_1 + d_2; \infty[$ that the computation of F_3 requires the calculation of a 2-D integral. For $x \gg d_1 + d_2$ (far from the island), it would be interesting to have a simpler form to quantify the level difference on the attenuation function obtained from homogeneous and inhomogeneous surfaces. Bremmer then showed for $x \gg d_1 + d_2$ that

$$F_3(x)/\sqrt{x} \approx w_3(x) \left[\frac{\alpha_3}{\alpha_1} - \frac{\alpha_3 \beta_{21}}{\alpha_1^2 \alpha_2} G_1(d_1) - \frac{\beta_{32}}{\alpha_1 \alpha_2} G_1(d_2) - \frac{\beta_{12}\beta_{23}}{\alpha_2} \int_{d_1}^{d_1+d_2} w_1(\xi) G_2(d_2 - \xi)\, d\xi \right] \tag{16}$$

where

$$G_i(x) = \frac{1 - F_i(v)}{\sqrt{x}} \quad \text{and} \quad G_i(0) = \alpha_i \sqrt{-\pi}. \tag{17}$$

Thus, for $\Delta_3 = \Delta_1$, one obtains

$$F_3(x)/\sqrt{x} \approx w_1(x) \left\{ 1 + \frac{\beta_{12}}{\alpha_1 \alpha_2} [G_1(d_1) - G_1(d_2)] + \frac{\beta_{12}^2}{\alpha_2} \int_{d_1}^{d_1+d_2} w_1(\xi) G_2(d_2 - \xi)\, d\xi \right\}. \tag{18}$$

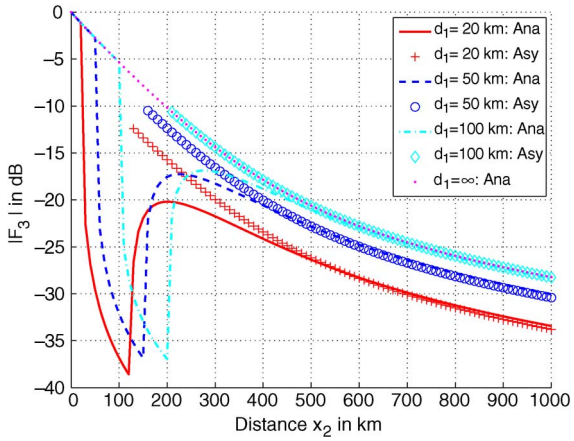

Fig. 11. $|F_3|$ versus the distance $x_2 = x - x_0$ in kilometers for a rough sea surface. The parameters are given in Table III.

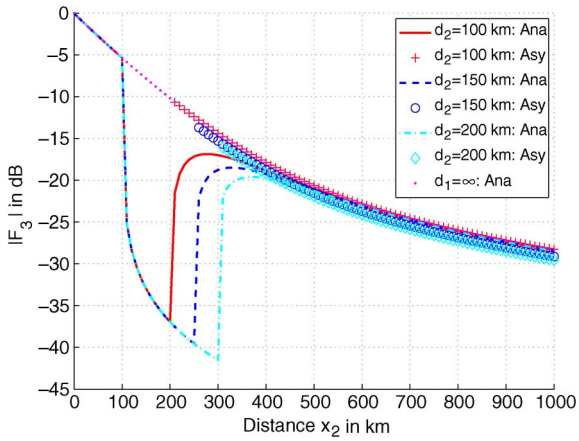

Fig. 12. Same as in Fig. 11.

TABLE III
PARAMETERS USED FOR FIGS. 11 AND 12 AND FOR THE CASE OF A SMOOTH SEA SURFACE WITH $z_0 = 0$ m AND $x_0 = 0$ m. THE SYMBOL "-" MEANS THAT THE CORRESPONDING PARAMETER CHANGES, AND IT IS GIVEN IN THE LEGEND OF THE CORRESPONDING FIGURE

Fig.	f (MHz)	z m	$(\epsilon_{r2}, \sigma_2)$ (S/m,-)	h_2 m	d_2 km	d_1 km
11	10	0	(0.01,30)	0	100	-
12	10	0	(0.01,30)	0	-	100

The terms after "1" are related to the Millington recovery effect since they vanish for a homogeneous surface. They are independent of the distance x. From the aforementioned equations, it is then easy to calculate numerically the level difference obtained far from the island between homogeneous and inhomogeneous surfaces.

For Figs. 11 and 12, the parameters are reported in Table III. In addition, in the legend, the label "Asy" means that F_3 is computed from (18) for $x \geq d_1 + d_2$, and $d_1 = \infty$ corresponds to a homogeneous sea surface.

As we can see in Fig. 11, for observation distances x that are far from the island, the curves match well. Moreover, as the distance d_1 increases, the recovery effect is more significant since the difference between the curves of homogeneous and inhomogeneous surfaces decreases. Indeed, for $d_1 = \{20, 50, 100\}$ km, $\Delta F_3|_{x=1000\,\mathrm{km}} = \{-5.2, -1.8, -0.2\}$ dB, in which $\Delta F_3 = F_3^{\mathrm{Ana}}/[F_3^{\mathrm{Ana}}|_{d_1=\infty}]$. Fig. 12 shows that the length d_2 of the island has a minor impact on the recovery effect since $\Delta F_3|_{x=1000\,\mathrm{km}} = \{-0.16, -0.21, -0.24\}$ dB. Thus, d_1 has a more important influence on the recovery effect than d_2.

V. CONCLUSION

In this paper, a detailed analysis of the ground wave propagation along an inhomogeneous rough surface in the HF band has been investigated from an efficient rigorous numerical method, called BMIA-CAG, and from an analytical approach, based on the work of Bremmer combined with the works of Barrick, to take into account the sea roughness. The Earth curvature is assumed to be negligible, and the case of a surface made up of three sections has been investigated to model the ground wave propagation above mixed sea–island–sea paths. For the heights of the transmitter and receiver, which are small in comparison to the wavelength and for a smooth surface, a very good agreement is obtained between both formulations, validating the Bremmer approach. In addition, the Millington recovery effect is predicted and studied with respect to the lengths of the first and second sections, the permittivity of the second section, the frequency, and the island height.

The Bremmer analytical equation is expressed from the attenuation functions of single homogeneous surfaces. Thus, from the theoretical works of Ishimaru *et al.* and Barrick done for a homogeneous rough surface, the sea roughness is taken into account by substituting the smooth surface normalized impedance for the rough one given by Barrick. The numerical results then showed a satisfactory agreement between both formulations. A prospect of this paper is to include the effect of the Earth curvature in the ground wave propagation, as done theoretically by Bremmer [22], Hufford [13], and Bourlier and Kubické [23] for a homogeneous smooth surface.

APPENDIX
INTEGRAL EQUATION VERIFIED BY THE ATTENUATION FUNCTION

For a 1-D surface, the total field $\psi(\mathbf{r})$ and its normal derivative $\partial\psi(\mathbf{r})/\partial n_s$ on the surface satisfied for $\mathbf{r}' \in (\Omega_0 \cup S)$ (upper medium Ω_0 plus surface S), the following integral equation [18]:

$$\psi(\mathbf{r}') = \psi_i(\mathbf{r}') + \int_S \left[\psi(\mathbf{r})\frac{\partial g_0(\mathbf{r},\mathbf{r}')}{\partial n_s} - \frac{\partial\psi(\mathbf{r})}{\partial n_s} g_0(\mathbf{r},\mathbf{r}')\right] dS. \tag{A1}$$

The scalar Green function of the upper medium is defined as $g_0 = g(\mathbf{r},\mathbf{r}') = (j/4)H_0^{(1)}(k_0\|\mathbf{r}-\mathbf{r}'\|)$, and $\psi_i(\mathbf{r}')$ is the incident field illuminating the surface. The function $H_0^{(1)}$ is the Hankel function of the zeroth order and of the first kind, and $k_0 = 2\pi/\lambda_0$ is the incident wavenumber. $\mathbf{r} = x\hat{\mathbf{x}} + z\hat{\mathbf{z}} = (x, z)$ is a point on the surface, and $\mathbf{r}' = x'\hat{\mathbf{x}} + z'\hat{\mathbf{z}} = (x', z')$ is the observation point. $\hat{\mathbf{x}}$ and $\hat{\mathbf{z}}$ are unitary vectors in Cartesian

coordinates. In (A1), the Cauchy principal value of the integral, defined as $\mathbf{r}=\mathbf{r}'$, is $\psi(\mathbf{r}')/2$. Thus, for $\mathbf{r}'\in\Omega_0$, (A1) becomes

$$\frac{\psi(\mathbf{r}')}{2}=\psi_i(\mathbf{r}')+\int\!\!\!\!\!\!\diagup_S\left[\psi(\mathbf{r})\frac{\partial g_0(\mathbf{r},\mathbf{r}')}{\partial n_s}-\frac{\partial\psi(\mathbf{r})}{\partial n_s}g_0(\mathbf{r},\mathbf{r}')\right]dS. \tag{A2}$$

Since the surface is assumed to be highly conducting ($|n|\gg 1$), the IBC (also named the Leontovitch boundary condition) approximation can be applied. This leads, on the surface for the TM polarization, to $\partial\psi(\mathbf{r})/\partial n_s=-j\Delta k_0\psi(\mathbf{r})$, where Δ is the surface normalized impedance defined as $\Delta=\sqrt{1-1/n^2}/n$, in which n is the refraction index. The only unknown is now the field $\psi(\mathbf{r})$, and from (A2), one obtains

$$\frac{\psi(\mathbf{r}')}{2}=\psi_i(\mathbf{r}')+\int\!\!\!\!\!\!\diagup_S\psi(\mathbf{r})\left[\frac{\partial g_0(\mathbf{r},\mathbf{r}')}{\partial n_s}+j\Delta k_0 g_0(\mathbf{r},\mathbf{r}')\right]dS \tag{A3}$$

where

$$\begin{aligned}\partial g_0(\mathbf{r},\mathbf{r}')\partial n_s&=\boldsymbol{\nabla}_{\mathbf{r}}g_0(\mathbf{r},\mathbf{r}')\cdot\hat{\mathbf{n}}_s\\&=-\frac{jk_0}{4}\frac{H_1^{(1)}(k_0\|\mathbf{r}-\mathbf{r}'\|)}{\|\mathbf{r}-\mathbf{r}'\|}(\mathbf{r}-\mathbf{r}')\cdot\hat{\mathbf{n}}_s\end{aligned} \tag{A4}$$

where $\hat{\mathbf{n}}_s=(-\gamma\hat{\mathbf{x}}+\hat{\mathbf{z}})/\sqrt{1+\gamma^2}$ is the unitary vector normal to the surface at the point $\mathbf{r}$, in which $\gamma=dz/dx$ is the surface slope.

Assuming that $k_0\|\mathbf{r}-\mathbf{r}'\|\gg 1$, the Green function can be expanded as

$$g_0(\mathbf{r},\mathbf{r}')=g_0^{\infty}(\mathbf{r},\mathbf{r}')=\frac{j}{4}\sqrt{\frac{2}{\pi k_0\|\mathbf{r}-\mathbf{r}'\|}}e^{j(k_0\|\mathbf{r}-\mathbf{r}'\|-\pi/4)} \tag{A5}$$

and since $H_1^{(1)}(u)\approx -jH_0^{(1)}(u)$ for $u\gg 1$, one obtains

$$\frac{\partial g_0(\mathbf{r},\mathbf{r}')}{\partial n_s}=jk_0g_0^{\infty}(\mathbf{r},\mathbf{r}')\frac{\mathbf{r}-\mathbf{r}'}{\|\mathbf{r}-\mathbf{r}'\|}\cdot\hat{\mathbf{n}}_s. \tag{A6}$$

The substitution of (A5) and (A6) into (A3) leads then to

$$\begin{aligned}\frac{\psi(\mathbf{r}')}{2}&=\psi_i(\mathbf{r}')+jk_0\int\!\!\!\!\!\!\diagup_S\psi(\mathbf{r})g_0^{\infty}(\mathbf{r},\mathbf{r}')\\&\quad\times\left[\Delta\sqrt{1+\gamma^2}-\frac{\gamma\,(x-x')-(z-z')}{\sqrt{(x-x')^2+(z-z')^2}}\right]dx\end{aligned} \tag{A7}$$

where $dS=dx\sqrt{1+\gamma^2}$.

For more clarity, the points $T(0,z_0)$, $Q(\xi,z_\xi)$, and $R(x,z)$ are defined and stand for the position of the transmitter, a point on the surface, and the position of the receiver, respectively (see Fig. 1). Assuming that $k_0QR\gg 1$, with the new notations, the aforementioned equation becomes

$$\begin{aligned}\frac{\psi(R)}{2}&=\psi_i(R)+jk_0\int\!\!\!\!\!\!\diagup_S\psi(Q)g_0^{\infty}(QR)\\&\quad\times\left[\Delta\sqrt{1+\gamma^2}-\frac{\gamma(\xi-x)-(z_\xi-z)}{QR}\right]d\xi\end{aligned} \tag{A8}$$

where QR is the distance between the points Q and R.

The attenuation function is defined as $\psi=2\psi_iF$. Substituting this equation into (A8) and dividing by $\psi_i(R)$, one obtains for $\psi_i(R)=g_0^{\infty}(TR)$ with $k_0TR\gg 1$

$$\begin{aligned}F(R)&=1+j2k_0\int\!\!\!\!\!\!\diagup_S F(Q)\frac{g_0^{\infty}(QR)g_0^{\infty}(TQ)}{g_0^{\infty}(TR)}\\&\quad\times\left[\Delta\sqrt{1+\gamma^2}-\frac{\gamma(\xi-x)-(z_\xi-z)}{QR}\right]d\xi.\end{aligned} \tag{A9}$$

The use of (A5) leads then to

$$\begin{aligned}F(x,z)=&1+\frac{j}{\sqrt{\pi}}\int_0^x F(\xi,z_\xi)\alpha(\xi)e^{jk_0(QR+TQ-TR)}\\&\times\sqrt{\frac{TR}{QR\times TQ}}\left[1-\frac{\gamma_\xi(\xi-x)-(z_\xi-z)}{\Delta(\xi)\sqrt{1+\gamma_\xi^2}QR}\right]\\&\times\sqrt{1+\gamma_\xi^2}d\xi\end{aligned} \tag{A10}$$

where $\alpha(\xi)=\Delta(\xi)\sqrt{jk_0/2}$ and $\gamma_\xi=\gamma(\xi)$. Moreover

$$\begin{cases}QR=\sqrt{(\xi-x)^2+(z_\xi-z)^2)}\\TQ=\sqrt{\xi^2+(z_\xi-z_0)^2}\\TR=\sqrt{x^2+(z-z_0)^2}.\end{cases} \tag{A11}$$

REFERENCES

[1] G. Millington, "Ground-wave propagation over an inhomogeneous smooth Earth," *Proc. Inst. Elect. Eng.*, vol. 96, no. 39, pp. 53–64, Jan. 1949.

[2] J. R. Wait, "The ancient and modern history of EM ground-wave propagation," *IEEE Antennas Propag. Mag.*, vol. 40, no. 5, pp. 7–24, Oct. 1998.

[3] R. E. Collin, "Hertzian dipole radiating over a lossy Earth or sea: Some early and late 20th-century controversies," *IEEE Antennas Propag. Mag.*, vol. 46, no. 2, pp. 64–79, Apr. 2004.

[4] C. Bourlier, G. Kubické, and Y. Brelet, "Rigorous prediction of the ground wave above flat and rough highly-conducting one-dimensional sea surfaces in VHF band," *IEEE Trans. Antennas Propag.*, vol. 59, no. 1, pp. 271–280, Jan. 2011.

[5] L. Tsang, C. H. Chang, and H. Sangani, "A banded matrix iterative approach to Monte Carlo simulations of scattering of waves by large scale random rough surface problems: TM case," *Electron. Lett.*, vol. 29, no. 2, pp. 166–167, Jan. 1993.

[6] D. E. Barrick, "Theory of HF and VHF propagation across the rough sea, 1, The effective surface impedance for a slightly rough highly conducting medium at grazing incidence," *Radio Sci.*, vol. 6, no. 5, pp. 517–526, 1971.

[7] D. E. Barrick, "Theory of HF and VHF propagation across the rough sea, 2, Application to HF and VHF propagation above the sea," *Radio Sci.*, vol. 6, no. 5, pp. 527–533, 1971.

[8] H. Bremmer, "The extension of Sommerfeld's formula for the propagation of radio waves over a flat Earth, to different conductivities of the soil," *Physica*, vol. 20, no. 1–6, pp. 441–460, 1954.

[9] G. Apaydin and L. Sevgi, "Numerical investigations of and path loss predictions for surface wave propagation over sea paths including hilly island transitions," *IEEE Trans. Antennas Propag.*, vol. 58, no. 4, pp. 1302–1314, Apr. 2010.

[10] G. Apaydin and L. Sevgi, "FEM-based surface wave multi-mixed-path propagator and path loss predictions," *IEEE Antennas Wireless Propag. Lett.*, vol. 8, pp. 1010–1013, 2009.

[11] Groundwave Propagation Curves for Frequencies Between 10 kHz and 30 MHz, ITU-R, Recommendations, P-368-7, Mar. 1992.

[12] L. Sevgi, "A mixed-path groundwave field strength prediction virtual tool for digital radio broadcast systems in medium and short wave bands," *IEEE Antennas Propag. Mag.*, vol. 48, no. 4, pp. 19–27, Aug. 2006.

[13] G. A. Hufford, "An integral equation approach to the problem of wave propagation over an irregular surface," *Q Appl. Math.*, vol. IX, no. 4, pp. 391–404, 1951.
[14] J. R. Wait, "Mixed path ground wave propagation: 1. Short distances," *J. Res. Nat. Bur. Stand.*, vol. 57, no. 1, pp. 1–15, Jul. 1956.
[15] J. R. Wait and L. C. Walters, "Curves for ground wave propagation over mixed land and sea paths," *IEEE Trans. Antennas Propag.*, vol. AP-11, no. 1, pp. 38–45, Jan. 1963.
[16] C. Bourlier and G. Berginc, "Microwave analytical backscattering models from randomly rough anisotropic sea surface—Comparison with experimental data in C and Ku bands," *Prog. Electromagn. Res.*, vol. 37, pp. 31–78, 2002.
[17] F. Harrington, *Field Computation by Moment Methods*. Piscataway, NJ: IEEE Press, 1993.
[18] L. Tsang, J. A. Kong, K.-H. Ding, and C. O. Ao, *Scattering of Electromagnetics Waves: Numerical Simulations*. New York: Wiley Interscience, 2001.
[19] N. Déchamps and C. Bourlier, "Electromagnetic scattering from a rough layer: Propagation-inside-layer expansion method combined to an updated BMIA/CAG approach," *IEEE Trans. Antennas Propag.*, vol. 55, no. 10, pp. 2790–2802, Oct. 2007.
[20] A. Ishimaru, J. D. Rockway, Y. Kuga, and S.-W. Lee, "Sommerfeld and Zenneck wave propagation for a finitely conducting one-dimensional rough surface," *IEEE Trans. Antennas Propag.*, vol. 48, no. 9, pp. 1475–1484, Sep. 2000.
[21] T. Elfouhaily, B. Chapron, K. Katsaros, and D. Vandermark, "A unified directional spectrum for long and short wind-driven waves," *J. Geophys. Res.*, vol. 102, no. C7, pp. 15 781–15 796, 1997.
[22] H. Bremmer, "Applications of operational calculus to ground-wave propagation, particularly for long waves," *IRE Trans. Antennas Propag.*, vol. 6, no. 3, pp. 267–272, Jul. 1958.
[23] C. Bourlier and G. Kubické, "HF ground wave propagation over a curved rough sea surface," *Waves Random Complex Media*, 2010, paper no. TWRM-2010-0016.R1, to be published.

Christophe Bourlier was born in La Flèche, France, on July 6, 1971. He received the M.S. degree in electronics from the University of Rennes, Rennes, France, in 1995 and the Ph.D. degree from the Système Electronique et Informatique Laboratory, Université de Nantes, in 1999.

While at the University of Rennes, he was with the Laboratory of Radiocommunication where he worked on antennas coupling in the VHF–HF band. He was an Assistant Researcher with the National Center for Scientific Research, where he worked on electromagnetic wave scattering from rough surfaces and objects for remote sensing applications. He is currently with the SEC Team, Institut de Recherche en Electrotechnique et Electronique de Nantes Atlantique Laboratory, Université Nantes Angers Le Mans, Polytech'Nantes, Nantes, France. He is the author of more than 130 journal articles and conference papers.

Gildas Kubické was born in Longjumeau, France, in September 1982. He received the Engineering degree and M.S. degree in electronics and electrical engineering in 2005 and the Ph.D. degree in 2008 from the Université de Nantes, Nantes, France.

He is currently a Research Engineer with the SEC Team, Institut de Recherche en Electrotechnique et Electronique de Nantes Atlantique Laboratory, Université Nantes Angers Le Mans, Polytech'Nantes. His research interests include electromagnetic scattering and radar-cross-section modeling.